RSC Advances

PAPER

Cite this: *RSC Adv.*, 2016, **6**, 18965

Influence of an oxygen vacancy on the electronic structure of the asymmetric mixed borate–carbonate $Pb_7O(OH)_3(CO_3)_3(BO_3)$†

A. H. Reshak*[ab] and Sushil Auluck[cd]

The influence of an oxygen vacancy on the electronic properties of a mixed borate–carbonate compound $Pb_7O(OH)_3(CO_3)_3(BO_3)$ is studied. We report calculations of the electronic band structure, the angular momentum resolved projected density of states and the valence electronic charge density distribution. The full-potential method within the generalized gradient approximation (PBE–GGA) and a recently modified Becke–Johnson potential (mBJ) shows an indirect band gap of 3.34 eV (PBE–GGA) and 3.56 eV (mBJ) for $Pb_7O(OH)_3(CO_3)_3(BO_3)$, while it is a direct gap of 1.10 eV (PBE–GGA) and 1.61 eV (mBJ) for the compound $Pb_7(OH)_3(CO_3)_3(BO_3)$ which has one O vacancy. Thus, the O vacancy causes a significant reduction in the band gap and also changes it from indirect to direct. The band gap reduction in $Pb_7(OH)_3(CO_3)_3(BO_3)$ is attributed to the appearance of new energy bands inside the energy gap of $Pb_7O(OH)_3(CO_3)_3(BO_3)$. The angular momentum resolved projected density of states for $Pb_7O(OH)_3(CO_3)_3(BO_3)$ and $Pb_7(OH)_3(CO_3)_3(BO_3)$ show that there exists a strong hybridization between B and O of the BO_3 group and between C and O of the CO_3 group. The valence electronic charge density for both compounds is presented. It reveals the origin of chemical bonding characteristics and the influence of the O vacancy. After a careful comparison, it is found that the crystal structure of $Pb_7O(OH)_3(CO_3)_3(BO_3)$ without an O vacancy can be considered as a parent phase of defect $Pb_7(OH)_3(CO_3)_3(BO_3)$.

Received 20th November 2015
Accepted 4th February 2016

DOI: 10.1039/c5ra24601f

www.rsc.org/advances

1. Introduction

Recently several carbonate non-centro-symmetric single crystals[1–4] have been synthesized because of their unusual structure and promising applications in optical and photonic devices, optical parametric oscillation (OPO), second harmonic generation (SHG) and laser frequency conversion.[5–18] Recently Maierhaba *et al.*[19] synthesized mixed borate–carbonate nonlinear optical materials which exhibit a large SHG response. They reported the first borate–carbonate ultra-violet (UV) nonlinear optical material with a chemical formula of $Pb_7O(OH)_3(CO_3)_3(BO_3)$. They attributed the large SHG to the strong interactions between the stereo-effect of Pb cations and co-parallel BO_3 and CO_3 triangles groups.[1–4,19,20] Maierhaba *et al.* have reported X-ray diffraction data and have measured the energy band gap. It has been found that $Pb_7O(OH)_3(CO_3)_3(BO_3)$ crystallizes in a non-centro-symmetric structure with hexagonal space group $P6_3mc$. The unit cell contains two formulas, the lattice parameters are reported to be $a = b = 10.519(16)$ Å and $c = 8.900(13)$ Å.[19] In addition, they have calculated the band structure and the density of states using CASTEP code within the generalized gradient approximation (PBE–GGA).[21] The CASTEP code is a non-full potential method which ignores the potential in the interstitial region. Moreover PBE–GGA underestimates the band gap. We would like to emphasize that in full-potential methods the potential and charge density are expanded into lattice harmonics inside each atomic sphere and as a Fourier series in the interstitial region. Hence, the effect of the full potential on the electronic properties can be ascertained. In addition, we have explored the effect of introducing one oxygen vacancy on the electronic properties. Thus the new compound is $Pb_7(OH)_3(CO_3)_3(BO_3)$. We call the original compound as I and the compound with oxygen vacancy as II. The mixed borate–carbonate $Pb_7O(OH)_3(CO_3)_3(BO_3)$ is newly synthesized compound and hence no details information regarding the electronic band structure and the total and the angular momentum resolved projected density of states. This motivated us to perform comprehensive theoretical calculations to ascertain the influence of an oxygen vacancy on the electronic properties. We thought it would be interesting to perform full potential calculation within the recently modified Becke–Johnson potential

[a]*New Technologies-Research Centre, University of West Bohemia, Univerzitni 8, 306 14 Pilsen, Czech republic. E-mail: maalidph@yahoo.co.uk*

[b]*Center of Excellence Geopolymer and Green Technology, School of Material Engineering, University Malaysia Perlis, 01007 Kangar, Perlis, Malaysia*

[c]*Council of Scientific and Industrial Research-National Physical Laboratory Dr K S Krishnan Marg, New Delhi 110012, India*

[d]*Department of Physics, Indian Institute of Technology Delhi, Hauz Khas, New Delhi 110016, India*

† Electronic supplementary information (ESI) available. See DOI: 10.1039/c5ra24601f

(mBJ),[22] to calculate the electronic band structure, density of states, the valence electronic charge density distribution and the chemical bonding characters of I and II compounds. The modified Becke–Johnson potential allows the calculation with accuracy similar to the very expensive GW calculations [221 000]. Hedin developed the GW method by linking 5 many-body equations together into a self-consistent scheme. The vertex correction arises from the two-particle Green's function (G) associated with the coulomb energy (W). It provides many-body corrections to the exchange and correlation energy. It is a local approximation to an atomic "exact-exchange" potential and a screening term.[22,23]

2. Calculation methodology

The calculations are performed based on the X-ray crystallographic data reported by Maierhaba's group[19] for the compound I. Then we have used the experimental crystallographic data of compound I and removed two oxygen atoms to investigate the influence of oxygen vacancy (as the unit cell has $Z = 2$) on the resulting properties. Therefore, a theoretical model originating from the designed oxygen vacancies has been proposed in order to seek the influence of O-vacancy on the band structure and the associated properties. The geometrical relaxation of I was achieved within the generalized gradient approximation (PBE–GGA)[21] using the full potential linear augmented plane wave (FPLAPW + lo) method as embodied in the WIEN2k code.[24] The resulting relaxed geometry of I is used to calculate the electronic structure and hence the associated properties using the recently modified Becke–Johnson potential (mBJ).[22] For II we removed the two O atoms. After the self consistent cycle the forces in I and II were similar. The crystal structures of I and II along with the unit cell are presented in Fig. 1 where the oxygen vacancies are clearly shown. The optimized atomic positions of I are listed in Table 1 in comparison with the experimental data of I.[19]

The muffin-tin radii (R_{MT}) of the atoms are chosen in such a way that the spheres did not overlap. The value of R_{MT} is taken to be 2.32 au. for Pb, 1.19 au. for O, 1.23 au. for B, 1.18 au. for C and 0.64 au. for H for both I and II. To achieve the total energy convergence, the basis functions in the interstitial region (IR) were expanded up to $R_{MT} \times K_{max} = 7.0$ and inside the atomic spheres for the wave function. The maximum value of l was taken as $l_{max} = 10$, while the charge density is Fourier expanded up to $G_{max} = 12$ (au.)$^{-1}$. Self-consistency is obtained using 192 for I and 72 for II $\vec{k}$ points in the irreducible Brillouin zone

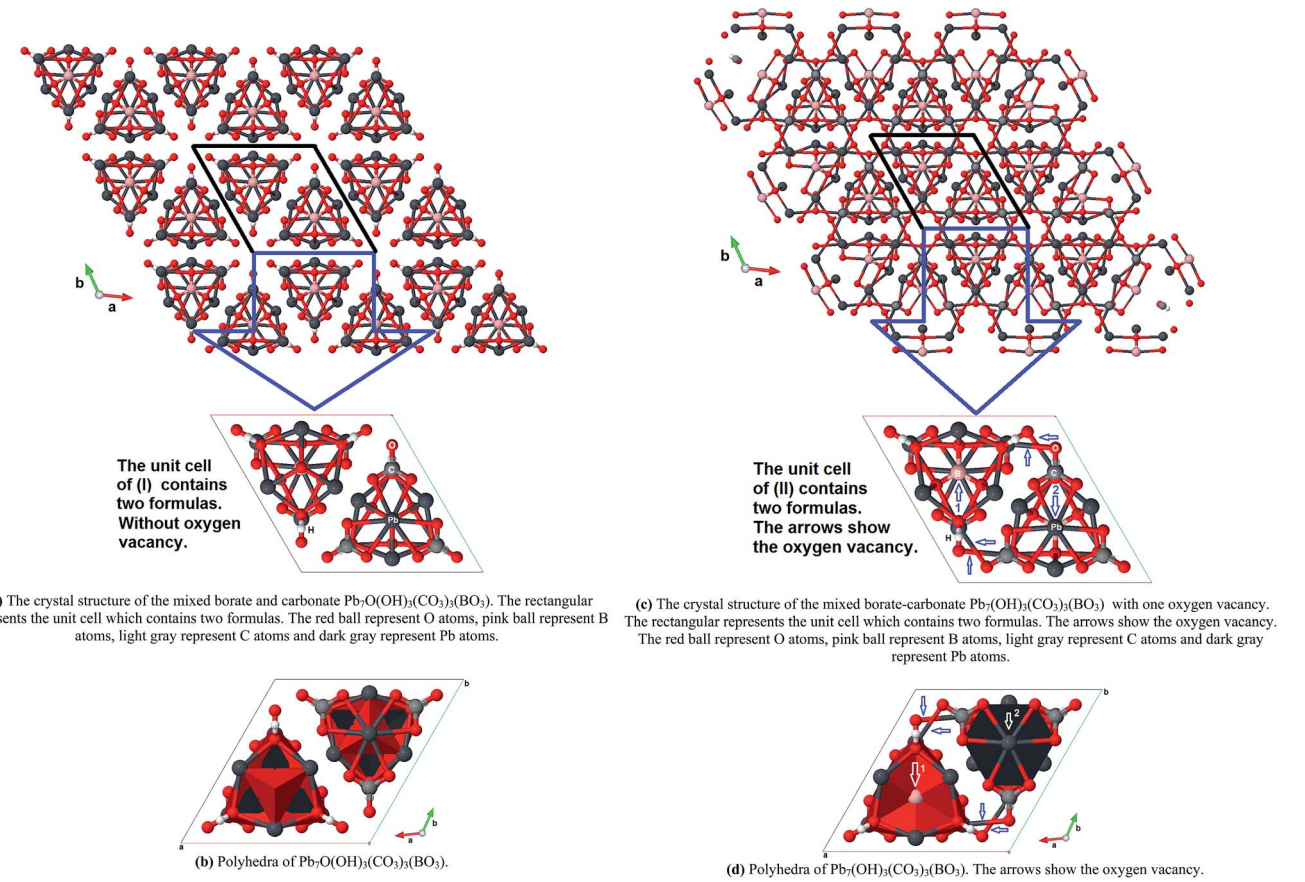

(a) The crystal structure of the mixed borate and carbonate $Pb_7O(OH)_3(CO_3)_3(BO_3)$. The rectangular represents the unit cell which contains two formulas. The red ball represent O atoms, pink ball represent B atoms, light gray represent C atoms and dark gray represent Pb atoms.

(c) The crystal structure of the mixed borate-carbonate $Pb_7(OH)_3(CO_3)_3(BO_3)$ with one oxygen vacancy. The rectangular represents the unit cell which contains two formulas. The arrows show the oxygen vacancy. The red ball represent O atoms, pink ball represent B atoms, light gray represent C atoms and dark gray represent Pb atoms.

(b) Polyhedra of $Pb_7O(OH)_3(CO_3)_3(BO_3)$.

(d) Polyhedra of $Pb_7(OH)_3(CO_3)_3(BO_3)$. The arrows show the oxygen vacancy.

Fig. 1 (a) The crystal structure of the mixed borate–carbonate $Pb_7O(OH)_3(CO_3)_3(BO_3)$. The rectangular represents the unit cell which contains two formulas. The red ball represent O atoms, pink ball represent B atoms, light gray represent C atoms and dark gray represent Pb atoms; (b) polyhedra of $Pb_7O(OH)_3(CO_3)_3(BO_3)$; (c) the crystal structure of the mixed borate–carbonate $Pb_7(OH)_3(CO_3)_3(BO_3)$ with one oxygen vacancy. The rectangular represents the unit cell which contains two formulas. The arrows show the oxygen vacancy. The red ball represent O atoms, pink ball represent B atoms, light gray represent C atoms and dark gray represent Pb atoms; (d) polyhedra of $Pb_7(OH)_3(CO_3)_3(BO_3)$. The arrows show the oxygen vacancy.

Table 1 Optimized atomic positions of $Pb_7O(OH)_3(CO_3)_3(BO_3)$ in comparison with the experimental data[19]

Atom	*x*-exp.	*x*-opt.	*y*-exp.	*y*-opt.	*z*-exp.	*z*-opt.
Pb(1)	0.3333	0.3333	0.6667	0.6667	0.2753(2)	0.2751
Pb(2)	0.6606(2)	0.6600	0.8303(1)	0.8301	0.8995(2)	0.8992
Pb(3)	0.4567(1)	0.4561	0.5433(1)	0.5431	0.6025(2)	0.6023
O(1)	0.3333	0.3333	0.6667	0.6667	0.5220(50)	0.5221
O(2)	0.6310(20)	0.6312	0.8154(12)	0.8152	0.6520(30)	0.6522
O(3)	0.4094(12)	0.4092	0.5906(12)	0.5904	0.8520(20)	0.8520
O(4)	0.8090(30)	0.8091	0.9045(13)	0.9043	0.3440(30)	0.3439
O(5)	0.5918(17)	0.5916	0.9014(19)	0.9012	0.3176(18)	0.3174
B(1)	0.3333	0.3333	0.6667	0.6667	0.8640(90)	0.8641
C(1)	0.6610(40)	0.6611	0.8310(20)	0.8311	0.3290(60)	0.3292
H	0.8615	0.8619	0.1379	0.1380	0.0941	0.0944

(IBZ). The self-consistent calculations are converged since the total energy of the system is stable within 0.00001 Ry. The electronic properties are calculated using a larger number of *k* points in the IBZ. It is well known that first-principles calculations are a powerful and useful tool to predict the crystal structure and its properties related to the electron configuration of a material before its synthesis.[25–28]

3. Results and discussion

3.1. Electronic band structures and density of states

The calculated electronic band structure along the high symmetry points of the first BZ and the angular momentum resolved projected density of states (PDOS) of oxygen atoms of I and II compounds are shown in Fig. 2(a) and (b). The valence

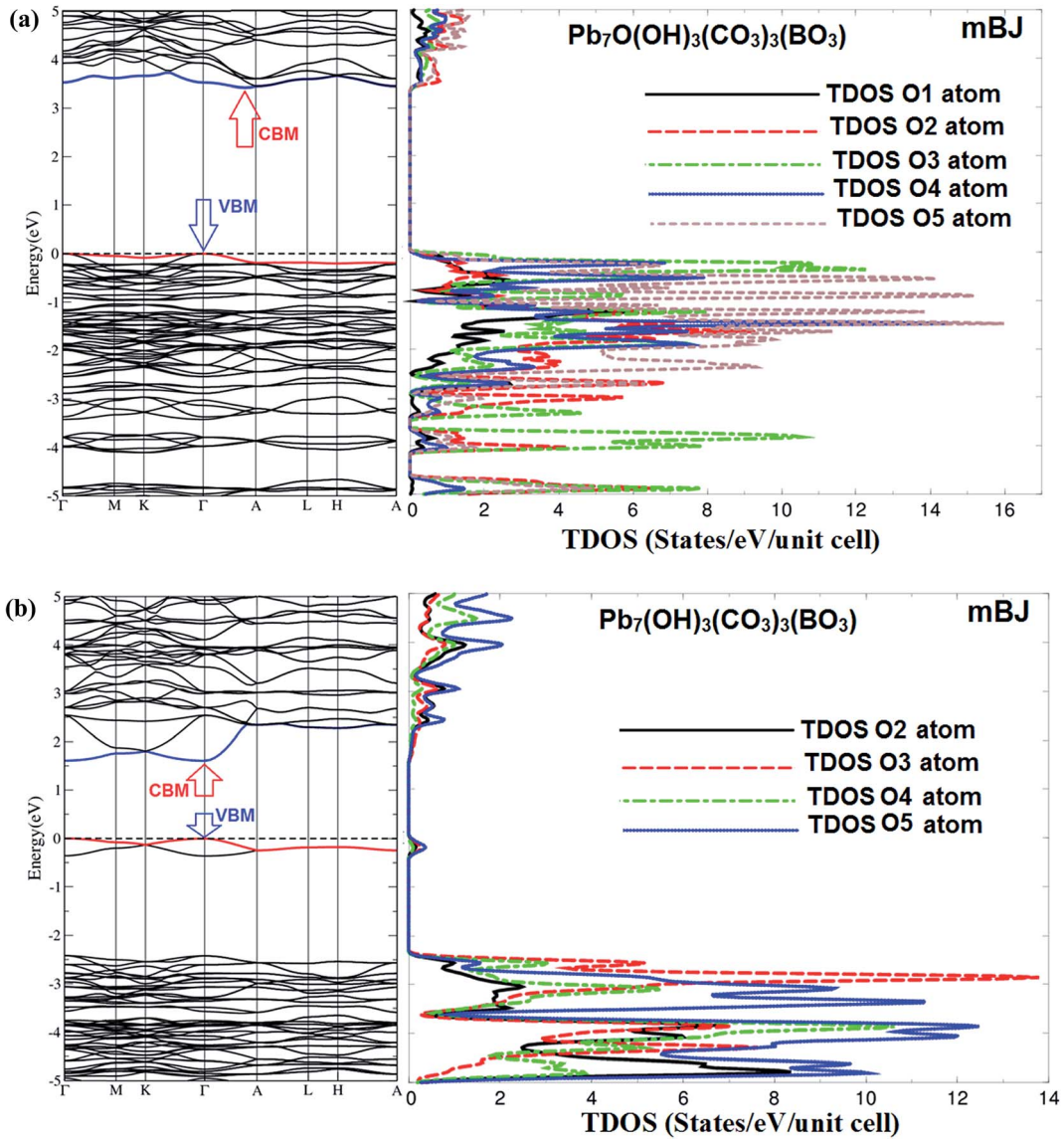

Fig. 2 The calculated electronic band structure of the mixed borate and carbonate $Pb_7O(OH)_3(CO_3)_3(BO_3)$ and $Pb_7(OH)_3(CO_3)_3(BO_3)$ along with the angular momentum resolved projected density of states (PDOS) of oxygen atoms of (I) and (II) crystals using LDA–mBJ. Total density of states is for unit cell ($Z = 2$) that is 2 formula units. Partial density of states is for one atom.

band maximum (VBM) of I and II is located at the center (Γ) of the BZ while the conduction band minimum (CBM) of I is situated between Γ and A points of BZ, resulting in an indirect energy band gap of 3.34 eV (PBE–GGA) and 3.56 eV (mBJ). The CBM of II is located at Γ of the BZ, resulting in a direct band gap of 1.10 eV (PBE–GGA) and 1.61 eV (mBJ). The band gap reduction in II is attributed to the appearance of a new energy bands within the energy gap region of I. Thus, the O-vacancy causes to reduce and tune the band gap and it changes the energy gap from indirect to direct. It has been found that mBJ succeeds by large amount in bringing the calculated energy gap of I close to the experimental one (3.65 eV)[19] as is expected from this approach.[29–31] Therefore, in the following, we show only the results obtained by mBJ. The angular momentum resolved projected density of states of I and II are presented in Fig. 3. The crystal structure of I and II consist of three Pb atoms and one atom of B, C and H. There are five O atoms in I and four O atoms in II. We illustrate the contribution of each atom in Fig. 3(a, c, e, g and i) for I and Fig. 3(b, d, f, h and j) for II. It is clear that the three Pb atoms and five O atoms in I and four O atoms in II exhibit different contributions while Pb_3 in I Pb_1 in II and O_5 in I and O_2 in II exhibit the highest contributions. Total density of states is for unit cell ($Z = 2$) that is 2 formula units. Partial density of states is for one atom. To explore the contribution of the orbitals we have decided to show the orbitals of one atom of each type, the one which shows highest contribution, for instance Pb_3-6s/6p/5d/4f (Pb_1-6s/6p/5d/4f), O_5-2s/2p (O_2-2s/2p), B-2s/2p, C-2s/2p and H-1s as shown in Fig. 3(g)–(j). The PDOS shows the influence of the oxygen vacancies on the bands dispersion. It is clear that in the VB of I, there is high density state region situated between −2.5 eV and Fermi level (E_F) which belongs to a O atom (Fig. 2(a)), and this feature vanishes from the electronic band structure of II (Fig. 2(b)) due to the oxygen vacancy. From the PDOS (Fig. 3(a)–(f)), it has been noticed that for I the VBM is mainly formed by O_3, O_4, O_5 and Pb_2, Pb_3 atoms while for II it is clear that the O bands are vanished confirming that the two oxygen vacancies keeping the VBM with Pb_1 and Pb_3 only. It is clear that the O vacancies push Pb_1 states which are situated below VBM towards Pb_3 to form the VBM while it pushes Pb_2 and the rest of Pb_1, Pb_3 states towards lower energies by around 2.0 eV. It is interesting to mention that there is a energy bands appeared directly above E_F in the forbidden gap, which composed of O_2-2p states. This could be called intermediate band (IB). The appearance of new bands may cause the appearance of new excitations. Recently, Ding *et al.*[32] reported that the position of such local energy level is changed due to the variation of oxygen vacancy concentration. There exists a strong hybridization between Pb_1, Pb_2 and Pb_3 atoms, also between O_1, O_2, O_3, O_4 and O_5 atoms. Furthermore, C atom hybridized with Pb_2, B with Pb_3, O_4 with Pb_3, O_5 with Pb_2 and Pb_3. The degree of the hybridization favors to enhance the strength of the covalent bonding. Fig. S1a and b (ESI†) shows the total density of states (TDOS) along with the electronic band structure and the first BZ are shown for I and II. It is clear that the oxygen vacancy significantly influences the TDOS.

The origin of chemical bonding can be elucidated from the angular momentum decomposition of the atoms projected

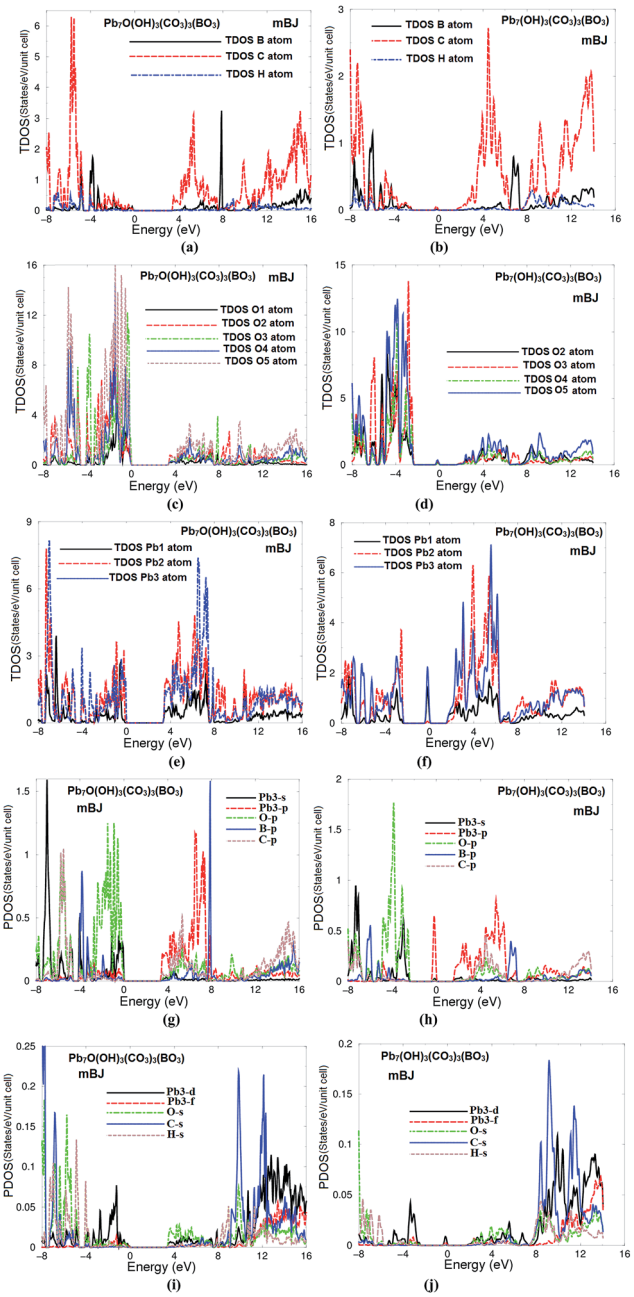

Fig. 3 (a, c, e, g and i) Calculated partial density of states (states/eV/unit cell) of the mixed borate and carbonate $Pb_7O(OH)_3(CO_3)_3(BO_3)$ using LDA–mBJ; (b, d, f, h and j) calculated partial density of states (states/eV/unit cell) of the mixed borate and carbonate $Pb_7(OH)_3(CO_3)_3(BO_3)$ using LDA–mBJ.

electronic density of states (Fig. 3(a)–(f)). Integrating the latter from −6.0 eV up to Fermi level (E_F) we obtain the total number of electrons per eV (e eV^{-1}) for the orbitals in each atom of I(II), Pb_1 atom 3.8(1.8) e eV^{-1}, Pb_2 atom 7.8(3.9) e eV^{-1}, Pb_3 9.2(2.3) e eV^{-1}, O_1 atom 6.0 e eV^{-1}, O_2 atom 9.0(8.0) e eV^{-1}, O_3 atom 12.0(13.5) e eV^{-1}, O_4 atom 14.5(11.0) e eV^{-1}, O_5 atom 16.0(12.5) e eV^{-1}, C atom 6.0(2.4) e eV^{-1}, B atom 1.8(1.2) e eV^{-1} and H atom 0.6(0.3) e eV^{-1}. The contributions of these atoms to the valence bands show that there is a clear influence on the electronic structure due to O vacancy. Also it is indicated that

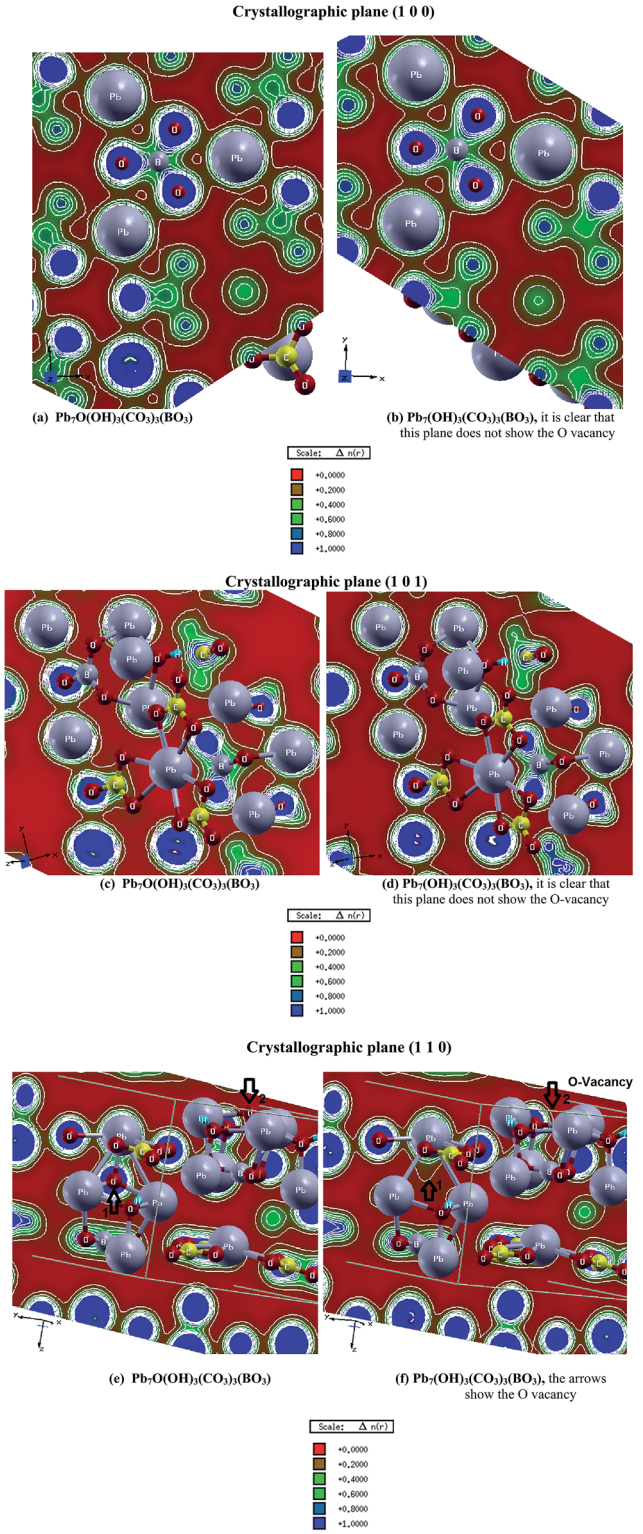

Fig. 4 The electron charge density distribution of the mixed borate and carbonate $Pb_7O(OH)_3(CO_3)_3(BO_3)$ and $Pb_7(OH)_3(CO_3)_3(BO_3)$ were calculated for; (a) (1 0 0) crystallographic plane of $Pb_7O(OH)_3(CO_3)_3(BO_3)$; (b) (1 0 0) crystallographic plane of $Pb_7(OH)_3(CO_3)_3(BO_3)$, it is clear that the (1 0 0) plane for $Pb_7(OH)_3(CO_3)_3(BO_3)$ does not show the O vacancy; (c) (1 0 1) crystallographic plane of $Pb_7O(OH)_3(CO_3)_3(BO_3)$; (d) (1 0 1) crystallographic plane of $Pb_7(OH)_3(CO_3)_3(BO_3)$, it is clear that the (1 0 1) plane for $Pb_7(OH)_3(CO_3)_3(BO_3)$ does not show the O vacancy; (e) (1 1 0) crystallographic plane of $Pb_7O(OH)_3(CO_3)_3(BO_3)$; (f) (1 1 0) crystallographic plane of $Pb_7(OH)_3(CO_3)_3(BO_3)$, the arrows show the oxygen vacancy.

Table 2 Calculated bond lengths (Å) of $Pb_7O(OH)_3(CO_3)_3(BO_3)$ in comparison with the experimental data[19a]

Bond	Exp.	This work	Bond	Exp.	This work
Pb(1)–O(1)	2.19(4)	2.20	Pb(2)–O(4)^{h}	2.729(6)	2.730
Pb(1)–O(5)^{a}	2.630(17)	2.631	Pb(2)–O(4)^{i}	2.729(6)	2.730
Pb(1)–O(5)^{b}	2.630(18)	2.631	Pb(3)–O(1)	2.359(13)	2.358
Pb(1)–O(5)^{c}	2.630(17)	2.631	Pb(3)–O(3)	2.38(2)	2.39
Pb(1)–O(5)	2.630(17)	2.631	Pb(3)–O(2)	2.548(13)	2.547
Pb(1)–O(5)^{d}	2.630(18)	2.631	Pb(3)–O(2)^{e}	2.548(14)	2.547
Pb(1)–O(5)^{e}	2.630(17)	2.631	B(1)–O(3)	1.39(2)	1.38
Pb(2)–O(2)	2.22(2)	2.23	B(1)–O(3)^{e}	1.39(2)	1.38
Pb(2)–O(3)	2.619(5)	2.620	B(1)–O(3)^{b}	1.39(2)	1.38
Pb(2)–O(3)^{b}	2.619(6)	2.620	C(1)–O(4)	1.35(4)	1.36
Pb(2)–O(4)^{f}	2.729(6)	2.729	C(1)–O(5)	1.28(3)	1.29
Pb(2)–O(4)^{g}	2.729(7)	2.729	C(1)–O(5)^{d}	1.28(3)	1.29

^{a} Symmetry transformations used to generate equivalent atoms: (a) $-x+y, y, z$, (b) $-y+1, x-y+1, z$, (c) $-y+1, -x+1, z$, (d) $x, x-y+1, z$, (e) $-x+y, -x+1, z$, (f) $y, -x+y+1, z+1/2$, (g) $x-y+1, x, z+1/2$, (h) $x-y+1, x, z-1/2$, (i) $y, -x+y+1, z-1/2$.

some electrons from Pb, C, B, H and O atoms are transferred into valence bands and contribute in covalence interactions between the atoms. The covalent bond arises due to the degree of the hybridization and the electronegativity differences between the atoms. It is clear that there is an interaction of charges between the atoms due to the existence of the hybridization, showing that there is a strong/weak covalent bonding between these atoms. Thus the angular momentum decomposition of the atoms projected electronic density of states help us to analyze the nature of the bonds according to the classical chemical concept. This concept is very useful to classify compounds into different categories with respect to different chemical and physical properties.

3.2. Valence electronic charge density

To investigate the nature of the bonds and the interactions between the atoms we have taken a careful look at valence electronic charge density distribution of I and II in three crystallographic planes namely (1 0 0), (1 0 1) and (1 1 0) as shown in Fig. 4(a)–(f). It has been observed that the (1 0 0) plane of I and II show only Pb, B and O atoms (Fig. 4(a) and (b)). The Pb atoms are surrounded by a spherical charge indicating the ionic nature of these atoms. The existence of B atom between the three O atoms which forms the BO_3 group perturbs the contour of the three O atoms. According to Pauling scale the electro-negativity of Pb, B, O, C and H are 2.33, 2.04, 3.44, 2.55 and 2.20. Therefore, due to the electro-negativity difference between O and B atoms one can see the charge transfer towards O atoms as indicated by the blue color around O atoms (according to the thermoscale the blue color exhibits the maximum charge accumulation). It has been noticed that the B atom forms strong covalent bonds with the nearest three O atoms (BO_3 group). It is clear that the (1 0 0) plane for II does not show the O-vacancy.

Fig. 4(c) and (d) illustrates (1 0 1) crystallographic plane of I and II which shows all the atoms. It is clear that C atom form a strong covalent bond with the three O atoms (CO_3) group.

Table 3 Calculated bond angles (°) of $Pb_7O(OH)_3(CO_3)_3(BO_3)$ in comparison with the experimental data[19a]

Angles	Exp.	This work	Angles	Exp.	This work
O(1)–Pb(1)–O(5)^a	81.8(4)	81.79	O(5)^b–Pb(1)–O(5)^c	68.7(7)	68.71
O(1)–Pb(1)–O(5)^b	81.8(4)	81.79	O(5)–Pb(1)–O(5)^d	49.9(7)	49.91
O(1)–Pb(1)–O(5)^c	81.8(4)	81.79	O(5)^a–Pb(1)–O(5)^b	49.9(7)	49.91
O(1)–Pb(1)–O(5)	81.8(4)	81.79	O(5)^c–Pb(1)–O(5)^e	49.9(7)	49.91
O(1)–Pb(1)–O(5)^d	81.8(4)	81.79	O(2)–Pb(2)–O(3)	74.5(7)	74.49
O(1)–Pb(1)–O(5)^e	81.8(4)	81.79	O(2)–Pb(2)–O(3)^b	74.5(7)	74.49
O(5)^b–Pb(1)–O(5)	117.99(19)	117.98	O(3)–Pb(2)–O(3)^b	54.6(9)	54.7
O(5)^a–Pb(1)–O(5)^c	117.99(19)	117.98	O(2)–Pb(2)–O(4)^f	85.5(8)	85.6
O(5)^a–Pb(1)–O(5)^d	117.99(17)	117.98	O(4)^f–Pb(2)–O(4)^g	67.0(10)	67.1
O(5)^c–Pb(1)–O(5)^d	117.99(18)	117.98	O(3)^b–Pb(2)–O(4)^f	115.4(7)	115.4
O(5)^b–Pb(1)–O(5)^e	117.99(17)	117.98	O(3)–Pb(2)–O(4)^f	159.3(8)	159.4
O(5)–Pb(1)–O(5)^e	117.99(18)	117.98	O(3)^b–Pb(2)–O(4)^g	159.3(8)	159.4
O(5)^c–Pb(1)–O(5)	161.0(7)	161.0(7)	O(3)–Pb(2)–O(4)^g	115.4(7)	115.5
O(5)^b–Pb(1)–O(5)^d	161.0(7)	161.0(7)	O(2)–Pb(2)–O(4)^g	85.5(7)	85.4
O(5)^a–Pb(1)–O(5)^e	161.0(7)	161.0	O(1)–Pb(3)–O(3)	86.5(11)	86.4
O(5)^a–Pb(1)–O(5)	68.7(7)	68.6	O(1)–Pb(3)–O(2)	73.7(4)	73.8
O(5)^b–Pb(1)–O(5)^c	68.7(7)	68.6	O(1)–Pb(3)–O(2)^e	73.7(4)	73.8
O(3)^b–Pb(2)–O(4)^g	159.3(8)	159.4	O(3)–Pb(3)–O(2)	73.3(6)	73.2
O(3)–Pb(2)–O(4)^f	159.3(8)	159.4	O(3)–Pb(3)–O(2)^e	73.3(6)	73.2
O(3)–Pb(2)–O(4)^g	115.4(7)	115.3	O(2)–Pb(3)–O(2)^e	134.1(9)	134.2
O(3)^b–Pb(2)–O(4)^f	115.4(7)	115.3	O(5)^d–C(1)–O(5)	120.0(3)	120.1
O(3)^b–Pb(2)–O(3)	54.6(9)	54.7	O(5)^d–C(1)–O(4)	120.0(17)	120.1
O(3)^e–B(1)–O(3)^b	119.4(9)	119.5	O(5)–C(1)–O(4)	120.0(17)	120.1
O(3)^e–B(1)–O(3)	119.4(9)	119.5	O(3)^b–B(1)–O(3)	119.4(9)	119.3

^{a} Symmetry transformations used to generate equivalent atoms: (a) $-x+y, y, z$ (b) $-y+1, x-y+1, z$ (c) $-y+1, -x+1, z$, (d) $x, x-y+1, z$ (e) $-x+y, -x+1, z$ (f) $y, -x+y+1, z+1/2$, (g) $x-y+1, x, z+1/2$.

Therefore, there exists a strong covalent bond between C atom and the three O atoms (CO_3 group). The Pb atoms tend to form a very weak covalent bond with O atoms. The (1 0 1) crystallographic plane confirms that B atom perturbs the contour of the three O atoms. It is clear that the (1 0 1) plane for II does not show the O-vacancy. Therefore, we have calculated the valence electronic charge density distribution of I and II in the (1 1 0) plane as shown in Fig. 4(e) and (f).

We have labeled the O-vacancy by arrows 1 and 2 (see Fig. 4(e) and (f)). It is clear that Pb (Fig. 4(e)) form strong covalent bond with O at the location labeled by 1 (see Fig. 4(e)). This covalent bond is missing in Fig. 4(f) due to the O vacancy. Thus, O vacancy leads to connect Pb by six O atoms in II instead of seven O atoms in I. The calculated valence electronic charge density distribution supports our finding from the PDOS which states that there exists a strong hybridization between B and O atoms also between C and O atoms. The strong/weak hybridization may lead to form strong/weak covalent bonding. It is interesting to compare our calculated bond lengths and angles with the measured one.[19] This is given in Tables 2 and 3 which reveal that there is a good agreement between the theory and experiment.

After a careful comparison, it is found that the crystal structure of I without O vacancy (Fig. 1a and b) can be considered as a parent phase of defect II structure (Fig. 1c and d).

4. Conclusions

The electronic band structure, the angular momentum resolved projected density of states and the valence electronic charge density distribution of the mixed borate–carbonate I and II are reported. The full-potential method within the generalized gradient approximation (PBE–GGA) and the recently modified Becke–Johnson potential (mBJ) reveals the I structure possesses an indirect band gap of 3.34 eV (PBE–GGA) and 3.56 eV (mBJ), while it is direct gap of 1.10 eV (PBE–GGA) and 1.61 eV (mBJ) for the O vacancy II structure. Thus, the O-vacancy causes to reduce and tune the band gap from indirect to direct band gap. The band gap reduction in II is attributed to the appearance of a new energy bands in the band gap of I. The angular momentum resolved projected density of states for I and II show that there exists a strong hybridization between B and O of BO_3 group and also between C and O of CO_3 group. The calculated valence electronic charge density reveals the origin of chemical bonding character. It shows the influence of O vacancy on the resulting properties of II. After a careful comparison, it is found that the crystal structure of I can be considered as a parent phase of defect II.

Acknowledgements

The result was developed within the CENTEM project, reg. no. CZ.1.05/2.1.00/03.0088, cofunded by the ERDF as part of the Ministry of Education, Youth and Sports OP RDI programme and, in the follow-up sustainability stage, supported through CENTEM PLUS (LO1402) by financial means from the Ministry of Education, Youth and Sports under the "National Sustainability Programme I. Computational resources were provided by MetaCentrum (LM2010005) and CERIT-SC (CZ.1.05/3.2.00/08.0144) infrastructures. SA would like to thank CSIR-National

Physical Laboratory and Physics Department Indian Institute of Technology Delhi for support.

References

1 G. H. Zou, N. Ye, L. Huang and X. S. Lin, Alkaline-Alkaline Earth Fluoride Carbonate Crystals $ABCO_3F$ (A = K, Rb, Cs; B = Ca, Sr, Ba) as Nonlinear Optical Materials, *J. Am. Chem. Soc.*, 2011, **133**, 20001–20007.

2 G. H. Zou, L. Huang, N. Ye, C. S. Lin, W. D. Cheng and H. Huang, Designing a Deep-Ultraviolet Nonlinear Optical Material with a Large Second Harmonic Generation Response, *J. Am. Chem. Soc.*, 2013, **135**, 18560–18566.

3 T. T. Tran, P. S. Halasyamani and J. M. Rondinelli, Role of Acentric Displacements on the Crystal Structure and Second-Harmonic Generating Properties of $RbPbCO_3F$ and $CsPbCO_3F$, *Inorg. Chem.*, 2014, **53**, 6241–6251.

4 T. T. Tran and P. S. Halasyamani, New Fluoride Carbonates: Centrosymmetric $KPb_2(CO_3)_2F$ and Noncentrosymmetric $K_{2.70}Pb_{5.15}(CO_3)_5F_3$, *Inorg. Chem.*, 2013, **52**, 2466–2473.

5 Q. C. Wei, H. Gunter, K. Petri, R. Margit, H. Markus, H. Hubert and L. Gert, Effects of Gigapascal Level Pressure on Protein Structure and Function, *J. Phys. Chem. B*, 2012, **116**, 1100–1110.

6 P. S. Halasyamani and K. R. Poeppelmeier, *Chem. Mater.*, 1998, **10**, 2753–2769; P. S. Halasyamani, Asymmetric Cation Coordination in Oxide Materials: Influence of Lone-Pair Cations on the Intra-octahedral Distortion in d0 Transition Metals, *Chem. Mater.*, 2004, **16**, 3586–3592.

7 I. Chung, J. I. Jang, C. D. Malliakas, J. B. Ketterson and M. G. Kanatzidis, Strongly Nonlinear Optical Glass Fibers from Noncentrosymmetric Phase-Change Chalcogenide Materials, *J. Am. Chem. Soc.*, 2010, **132**, 384–389.

8 W. J. Yao, R. He, X. Y. Wang, Z. S. Lin and C. T. Chen, Analysis of Deep-UV Nonlinear Optical Borates: Approaching the End, *Adv. Opt. Mater.*, 2014, **2**, 411–417.

9 H. W. Huang, J. Y. Yao, Z. S. Lin, X. Y. Wang, R. He, W. J. Yao, N. X. Zhai and C. T. Chen, Molecular Engineering Design to Resolve the Layering Habit and Polymorphism Problems in Deep UV NLO Crystals: New Structures in $MM'Be_2B_2O_6F$ (M=Na, M′=Ca; M=K, M′=Ca, Sr), *Chem. Mater.*, 2011, **23**, 5457–5463.

10 L. Y. Li, G. B. Li, Y. X. Wang, F. H. Liao and J. H. Lin, Bismuth Borates: One-Dimensional Borate Chains and Nonlinear Optical Properties, *Chem. Mater.*, 2005, **17**, 4174–4180.

11 G.-J. Cao, J. Lin, J.-Y. Wang, S.-T. Zheng, W.-H. Fang and G.-Y. Yang, Two additive-induced isomeric aluminoborates templated by methylamine, *Dalton Trans.*, 2010, **39**, 8631–8636.

12 M. D. Donakowski, R. Gautier, J. Yeon, D. T. Moore, J. C. Nino, P. S. Halasyamani and K. R. Poeppelmeier, The Role of Polar, Lamdba (Λ)-Shaped Building Units in Noncentrosymmetric Inorganic Structures, *J. Am. Chem. Soc.*, 2012, **134**, 7679–7689.

13 C. F. Sun, C. L. Hu, X. Xu, B. P. Yang and J. G. Mao, Explorations of New Second-Order Nonlinear Optical Materials in the Potassium Vanadyl Iodate System, *J. Am. Chem. Soc.*, 2011, **133**, 5561–5572.

14 H. S. Hu, F. Wei, X. F. Wang, L. Andrews and J. Li, Actinide–Silicon Multiradical Bonding: Infrared Spectra and Electronic Structures of the Si(μ-X) AnF_3 (An = Th, U; X = H, F) Molecules, *J. Am. Chem. Soc.*, 2014, **136**, 1427–1437.

15 H. P. Wu, H. W. Yu, Z. H. Yang, X. L. Hou, X. Su, S. L. Pan, K. R. Poeppelmeier and J. M. Rondinelli, Designing a Deep-Ultraviolet Nonlinear Optical Material with a Large Second Harmonic Generation Response, *J. Am. Chem. Soc.*, 2013, **135**, 4215–4218.

16 S. J. Choyke, S. M. Blau, A. A. Larner, S. A. Narducci, J. Yeon, P. S. Halasyamani and A. Norquist, Noncentrosymmetry in New Templated Gallium Fluorophosphates, *J. Inorg. Chem.*, 2009, **48**, 11277–11282.

17 H. Q. Tan, S. C. Du, Y. F. Bi and W. P. Liao, Two Elongated Octahedral Coordination Cages Constructed by M4-TC4A Secondary Building Units (M = CoII and FeII) and 2,2′-Bipyridine-4,4′-dicarboxylic Acids, *Inorg. Chem.*, 2014, **53**, 7083–7085.

18 M.-H. Zeng, Z. Yin, Y.-X. Tan, W.-X. Zhang, Y.-P. He and M. Kurmoo, Nanoporous Cobalt(II) MOF Exhibiting Four Magnetic Ground States and Changes in Gas Sorption upon Post-Synthetic Modification, *J. Am. Chem. Soc.*, 2014, **136**, 4680–4688.

19 M. Abudoureheman, L. Wang, X. Zhang, H. Yu, Z. Yang, C. Lei, J. Han and S. Pan, $Pb_7O(OH)_3(CO_3)_3(BO_3)$: First Mixed Borate and Carbonate Nonlinear Optical Material Exhibiting Large Second-Harmonic Generation Response, *Inorg. Chem.*, 2015, **54**, 4138–4142.

20 H. W. Yu, H. P. Wu, S. L. Pan, Z. H. Yang, X. L. Hou, X. Su, Q. Jing, K. R. Poeppelmeier and J. M. Rondinelli, $Cs_3Zn_6B_9O_{21}$: A Chemically Benign Member of the KBBF Family Exhibiting the Largest Second Harmonic Generation Response, *J. Am. Chem. Soc.*, 2014, **136**, 1264–1267.

21 J. P. Perdew, K. Burke and M. Ernzerhof, Generalized Gradient Approximation Made Simple, *Phys. Rev. Lett.*, 1996, **77**, 3865–3868.

22 F. Tran and P. Blaha, Accurate Band Gaps of Semiconductors and Insulators with a Semilocal Exchange-Correlation Potential, *Phys. Rev. Lett.*, 2009, **102**, 226401.

23 L. Hedin, New Method for Calculating the One-Particle Green's Function with Application to the Electron-Gas Problem, *Phys. Rev.*, 1965, **139**, A796; L. Hedin and S. Lundqvist, *Solid State Physics*, ed. H. Ehrenreich, F. Seitz and D. Turnbull, Academic, New York, 1969, vol. 23; L. Hedin, Electron correlation: keeping close to an orbital description, *Int. J. Quantum Chem.*, 1995, **56**, 445–452.

24 P. Blaha, K. Schwarz, G. K. H. Madsen, D. Kvasnicka and J. Luitz, *WIEN2k, An augmented plane wave plus local orbitals program for calculating crystal properties*, Vienna University of Technology, Austria, 2001.

25 K. J. Plucinski, I. V. Kityk, J. Kasperczyk and B. Sahraoui, The structure and electronic properties of silicon oxynitride gate dielectrics, *Semicond. Sci. Technol.*, 2001, **16**, 467–470.

26 M. Malachowski, I. R. Kityk and B. Sahraoui, Electronic structure and optical response in $Ga_xAl_{1-x}N$ solid alloys, *Phys. Lett. A*, 1998, **242**, 337–342.

27 I. Fuks-Janczarek, R. Miedzinski, M. G. Brik, A. Majchrowski, L. R. Jaroszewicz and I. V. Kityk, Z-scan analysis and *ab initio* studies of β-$BaTeMo_2O_9$ single crystal, *Solid State Sci.*, 2014, **27**, 30–35.

28 A. H. Reshak, A. Majchrowski, M. Swirkowicz, A. Kłos, T. Łukasiewicz, I. V. Kityk, K. Iliopoulos, S. Couris and M. G. Brik, Optical features of calcium neodymium oxyborate $Ca_4NdO(BO_3)_3$ doped by Yb^{3+}, *J. Alloys Compd.*, 2009, **481**, 14–16.

29 A. H. Reshak, Specific features of electronic structures and optical susceptibilities of molybdenum oxide, *RSC Adv.*, 2015, **5**, 22044.

30 A. H. Reshak, H. Huang, H. Kamarudin and S. Auluck, Alkali–metal/alkaline-earth-metal fluorine beryllium borate $NaSr_3Be_3B_3O_9F_4$ with large nonlinear optical properties in the deep-ultraviolet region, *J. Appl. Phys.*, 2015, **117**, 085703.

31 A. H. Reshak, Transport properties of g-BC3 and t-BC3 phases, *RSC Adv.*, 2015, **5**, 33632.

32 B. F. Ding, H. J. Qian, C. Han, J. Y. Zhang, S. E. Lindquist, B. Wei and Z. L. Tang, Oxygen Vacancy Effect on Photoluminescence Properties of Self-Activated Yttrium Tungstate, *J. Phys. Chem. C*, 2014, **118**, 25633.

